A new testing procedure to quantify unfavourable environmental effect on mechanical performance of composite reinforcement system

Haji Akbar Sultani, Arvydas Rimkus, Aleksandr Sokolov and Viktor Gribniak

Laboratory of Innovative Building Structures,
Vilnius Gediminas Technical University,
Sauletekio av. 11, Vilnius LT-10223, Lithuania

Abstract

Current technology development ensures a variety of material types for reinforcing and strengthening concrete structures. However, the absence of a uniform testing methodology complicates quantification (and comparison) of the mechanical performance of the composite reinforcements. In addition, the necessity to quantify the long-term degradation of the mechanical resistance intricates the issue. This research employs the equivalent residual stiffness approach to measure structural performance. It adapts a recently developed testing layout and a simplified analytical model to analyse the residual flexural stiffness of standardised laboratory specimens. The developed analytical model explicitly relates the particular moment and curvature values, requiring neither iterative calculations nor the load history. This feature allows the comparative analysis and quantification of the residual stiffness of the repeatedly loaded composite elements with varied reinforcement materials' layouts. The previous short-term tests identified the efficiency of hybrid systems employing fibre-reinforced polymer (FRP) materials and steel bars. However, the FRP components can be vulnerable to ultraviolet radiation, humidity, freezing-thawing cycles, and elevated temperature. Thus, this study includes 34 composite beams subjected to the service load. After that, the reference specimens were stored in laboratory conditions; the alternative samples, exposed to the open air outside the building, estimated the environmental effect on the stiffness decay. This manuscript reports the partial results of the ongoing test program.

1 Introduction

The current reinforcing technologies provide various materials for strengthening concrete structures [1]. Fibre-reinforced polymers (FRP) are a promising reinforcement alternative to steel because of their high strength, lightweight, immunity to corrosion, and electromagnetic transparency [2]. Still, the relatively low resistance to ultraviolet radiation, high humidity, and elevated temperatures can degrade the mechanical performance of FRP materials with time [3], [4]. In addition, different types of FRP reinforcement systems, i.e. internal bars, near-surface mounted (NSM) strips, and externally bonded reinforcement (EBR) sheets, demonstrate diverse effects on the mechanical performances of the composite systems [5]. Studies [6], [7] showed that the FRP combination with steel reinforcement could effectively solve engineering problems. However, this research was motivated by the lack of a uniform comparative analysis approach to quantify the efficiency of the reinforcement systems, combining different materials.

This investigation aims to adapt the recently developed testing layout and a simplified analytical model [7] to analyse the residual flexural stiffness of standardised laboratory specimens. The research employs the equivalent residual stiffness approach to measure the structural performance of alternative composite reinforcement systems. The applied analytical model explicitly relates the particular moment and curvature values, quantifying the equivalent stresses acting in the concrete belonging to the tension zone. The calculations require neither iterative calculations nor the load history under the assumption of the rectangular distribution of the tensile stresses in the concrete. This assumption allows the comparative analysis and quantifying of the residual stiffness of the repeatedly loaded composite elements with varied reinforcement materials' layouts.

The considered beam specimens' cross-section was selected in the previous study [5] to satisfy the simplified modelling assumption (i.e. the rectangular distribution of stresses in the tensile concrete). In other words, the corresponding 'exact' tension-stiffening diagram [8] has a rectangular shape typical for slab-like flexural members. However, it is paramount to note that the simplified analytical model

does not define concrete's constitutive law. The equivalent stresses only estimate the residual flexural stiffness to analyse the long-term decay in the mechanical performance of the composite reinforcement.

This manuscript reports the partial results of the ongoing test program that employs 34 test samples with different arrangements and combinations of composite reinforcement. First, the beam samples were subjected to the service load. After that, the reference specimens were stored in laboratory conditions; the alternative elements, exposed to the open air outside the building, estimated the environmental effect on the stiffness decay. This manuscript reports the partial results of four beam specimens, illustrating the proposed analysis procedure.

2 Test setup

The previous studies [5], [7] developed the geometry of the bending test specimens—the experimental layout design focused on the setup's ability to form multiple cracks in a relatively small sample because of the laboratory equipment limitations. This condition diminishes the cracking effect, transforming the moment-curvature relationship into the stress-strain diagram via inverse analysis [8].

Thus, this study employs the 1000 mm long slab-shaped beams tested under the four-point bending scheme, as Figure 1 shows. Figure 2 demonstrates the experimental setup. The specimens were subjected to monotonically increasing and repeating loads using a 5 MN capacity servo-hydraulic testing machine under displacement control and the 0.4 mm/min loading speed. Linear variable displacement transducers (LVDT) and digital image correlation system (DIC) monitored deformations of the opposite sides of the beams denoted as "①" and "②" in Figures 1 and 2—the DIC system monitored the development of the cracks. However, the cracking analysis is beyond this study's scope; therefore, this presentation does not include these results. The LVDT L_1–L_3, L_4–L_6, and L_7–L_9 measured the vertical displacements, and the indicators L_{10}–L_{15} estimated deformations of the side surface ①. The data logger ALMEMO 5690-2 collected the load cell and LVDT outputs every second.

The 200 × 100 mm cross-section was reinforced with various combination of the internal bars, near-surface mounted strips and externally bonded sheets. Although this ongoing study employs 34 beams, this manuscript reports the partial results of only four beams. Table 1 describes the geometry and material properties of these beam specimens.

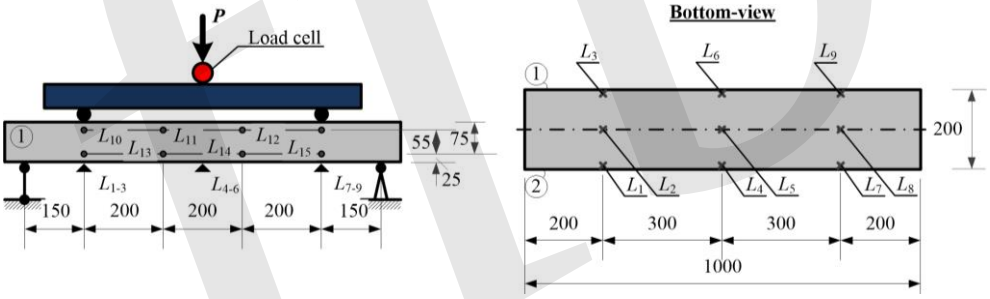

Fig. 1 The loading scheme and indicators' distribution.

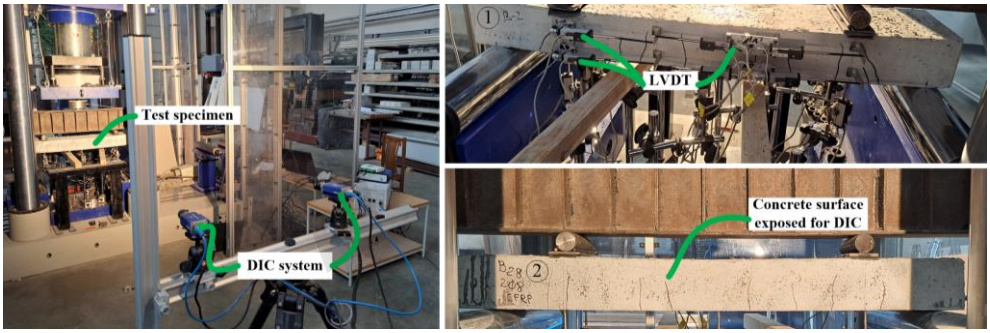

Fig. 2 The experimental setup.

Table 1 Geometry and material properties of the analysed beams.

Beam	h [mm]	b [mm]	d_1 [mm]	d_2 [mm]	A_{r1} [mm^2]	A_{r2} [mm^2]	E_{r1} [GPa]	E_{r2} [GPa]	f_{cm} [MPa]	t [days]
B1-NSM	103	199	93	-	28.0	-	170	-	48.1	120/274
B5-EBR	104	198	105	-	32.8	-	230	-	48.1	119/276
B11-NSM	103	200	93	-	28.0	-	170	-	60.5	116/273
B19-2x8-EBR	100	199	83	101	100.5	32.8	202	230	60.5	97/272

The selected specimens in Table 1 represent the NSM and EBR systems; the beam B19 combines two 8 mm steel bars, and a carbon FRP EBR sheet adhesively attached to the most tensioned bottom surface (Fig. 1). The unidirectional carbon MapeWrap C UNI-AX FRP sheets (the equivalent thickness of the dry material = 0.166 mm) were used as EBR. The NSM reinforcement system was composed of a pultruded 10×1.4 mm carbon FRP strip (S&P C-Laminate); the strips were installed in the 4×12 mm grooves milled at the bottom surface of the specimens. The two-component epoxy adhesive S&P Resin 220 filled these grooves before the strip installation. The adhesives of EBR and NSM systems were installed at least seven days before the mechanical tests to form a reliable adhesion contact between FRP materials and concrete. In Table 1, h and b denote the cross-section height and width; d_1 and d_2 stand for the effective depth of the reinforcement layers (internal bars and EBR sheet in beam B19), and the subscript numbers have the same meaning for the reinforcement area (A_r) and modulus of elasticity (E_r); f_{cm} is the compressive strength of the ∅150×300 mm concrete cylinder at the age of 87 days (specimens B1 and B5) and 84 days (samples B11 and B19). Table 1 also indicates the specimens' age (t) corresponding to the first and second testing stages.

The beam specimens were produced in two batches using laboratory-mixed concrete. The mix proportions for one cubic meter are following: the cement CEM I 42.5 R = 356 kg, water = 163 l, the limestone powder = 177 kg, the 0/4 mm sand = 890 kg, the 4/16 mm crushed dolomite aggregates = 801 kg, the superplasticiser Mapei Dynamon XTend = 1.97% (by the cement weight), and the admixture SCP 1000 Optimiser = 3.5 kg. The mixture also encompassed 0.9 kg of the Crackstop M Ultra synthetic micro-fibres and 4.2 kg of the Durus EasyFinish synthetic macro-fibres to avoid a sudden failure of the shear zone.

3 Analytical model for the inverse moment-curvature analysis

The previous study [7] verified the adequacy of this simplified analytical concept. Thus this manuscript presents only explanations necessary for the development of regression relationships, determining the environmental impact on the mechanical properties of the beam samples. The considered analytical model employs the following simplifications:

- The Euler-Bernoulli hypothesis is valid. An interested reader can find substantiation of this assumption for reinforced concrete beams elsewhere (e.g., [9], [10]).
- The concrete cracking process follows the smeared crack model. Numerous literature examples (e.g., [8], [10]) proved the adequacy of this assumption.
- Perfectly elastic deformation models describe the behaviour of all reinforcement materials and compressive concrete. This assumption substantially simplifies the analytical expressions, though non-linear material laws are feasible for iterative calculations. Reference [7] provides an example of such an analytical procedure.
- The tensile stresses in the concrete have a rectangular distribution, describing the equivalent stress value. This fundamental simplification explicitly relates the particular moment and curvature values, avoiding iterative calculations [5], [7]. Thus, quantifying the residual stiffness of the repeatedly loaded composite elements becomes possible.

Figure 3 shows the analytical model scheme, which employs the transformed section approach combining different reinforcement types (e.g., beam B19, Table 1) in one 'transformed' component (Fig. 3a). The following formulas define the corresponding effective depth d_r, area A_r, and modulus E_r:

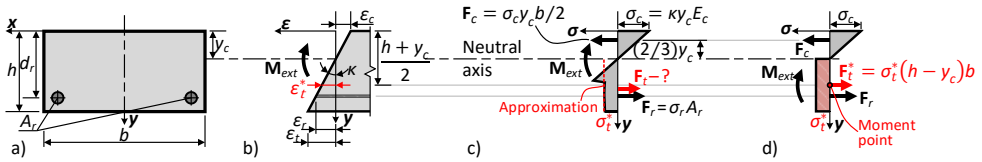

Fig. 3 Analytical model of the pure bending zone [7]: a) transformed cross-section; b) strain distribution; c) stress distribution; d) the equivalent stress approach.

$$d_r = \frac{\sum_{i=1}^{n} E_i A_i d_i}{\sum_{i=1}^{n} E_i A_i}, \quad A_r = \frac{1}{E_r}\sum_{i=1}^{n} E_i A_i, \quad E_r = E_1, \tag{1}$$

where E_i, A_i, and d_i are the modulus of elasticity, cross-section area, and effective depth of the i-th reinforcement layer; n is the number of reinforcement layers. The considered example (Table 1) shows the maximum number $n = 2$.

Figures 3b and 3c demonstrate the strain and strain distribution in the transformed section. The rectangular stress approximation defines the equivalent stress value (Fig. 3d), which is the further analysis object.

The following equilibrium equations of internal forces and bending moments for the centroid of the equivalent tensile stress diagram (Fig. 3d) determine the proposed residual stiffness model:

$$\mathbf{F}_t^* + \mathbf{F}_r - \mathbf{F}_c = 0, \tag{2a}$$

$$\mathbf{F}_r\left(d_r - \frac{h + y_c}{2}\right) + \mathbf{F}_c\left(\frac{h + y_c}{2} - \frac{y_c}{3}\right) - \mathbf{M}_{ext} = 0, \tag{2b}$$

where $\mathbf{F}_t^*$ is the equivalent resultant force in the tensile concrete; $\mathbf{F}_r$ and $\mathbf{F}_c$ are the internal forces acting on the tensile reinforcement and the compressive concrete; Figure 3 describes the remaining notations.

The solution of the above equation system relates the internal forces with corresponding stresses (Figs. 3c and 3d). In addition, it employs the strain compatibility condition (Fig. 3b). An interested reader can find detailed explanations in the article [7]. The resulting equation defines the third-order polynomial of the neutral axis ordinate y_c:

$$C_3 y_c^3 + C_2 y_c^2 + C_1 y_c + C_0 = 0 \tag{3a}$$

with coefficients

$$C_3 = \frac{E_c b}{6E_r A_r}, \quad C_2 = 1 + \frac{E_c bh}{2E_r A_r}, \quad C_1 = h - 3d_r, \quad C_0 = 2d_r^2 - hd_r - \frac{2\mathbf{M}_{ext}}{\kappa E_r A_r}. \tag{3b}$$

The polynomial (3a) has three roots, and the condition $0 < y_c \le h$ defines the neutral axis position:

$$y_c = \frac{1}{3C_3}\left\{2\sqrt{C_2^2 - 3C_3C_1}\cos\left(\frac{1}{3}\cos^{-1}\left\{-\frac{27C_3^2C_0 - 9C_3C_2C_1 + 2C_2^3}{2\sqrt{[C_2^2 - 3C_3C_1]^3}}\right\}\right) - C_2\right\}. \tag{4}$$

The following formulas express the equivalent stress (Fig. 3d) and corresponding strain (Fig. 3b):

$$\sigma_t^* = \kappa\frac{y_c^2 bE_c - 2(d_r - y_c)E_r A_r}{2(h - y_c)b}, \tag{5a}$$

$$\varepsilon_t^* = \kappa\frac{h - y_c}{2}. \tag{5b}$$

4 Beam tests and discussion of the results

This study analyses the environmental impact on the mechanical performance of the reinforced beams. Thus, the beam specimens experienced two testing stages. In the first stage, the beams were subjected to the service load conditions, corresponding to the 45% and 60% range of the ultimate bending resistance (determined by testing the identical beam sample until failure). The beams were loaded repeatedly (in five cycles), fluctuating the load within the boundaries mentioned to generate a reliable database. Then, the reference specimens were stored in laboratory conditions; the alternative samples were exposed to the open air outside the building. The same tests were repeated after approximately a half year. And the beams were returned to the past environmental conditions (until the next test round). For example, specimen B1 (Table 1) is stored in laboratory conditions, and the remaining three selected

samples are exposed to the open environment (outside the laboratory building). Figure 4 describes the environmental parameters; the average 35% relative humidity and 20.5 °C describe the laboratory conditions.

As Section 3 mentioned, the analytical model explicitly relates the moment and curvature values for deriving the equivalent stresses (Eqn. 5a). The further analysis employs the vertical displacement monitoring results of the pure bending zone (Fig. 1). The following equation determines the curvature:

$$\kappa = \frac{8 \cdot \delta}{l_b^2 + 4 \cdot \delta^2}, \quad \delta = \frac{\delta_4 + \delta_5 + \delta_6}{3} - \frac{\delta_1 + \delta_2 + \delta_3 + \delta_7 + \delta_8 + \delta_9}{6}, \tag{6}$$

where δ is the deflection over the pure bending zone; δ_i is the displacement obtained by LVDT L_i (i = 1…9, Fig. 1); l_b (= 600 mm) is the pure bending zone length. Figure 5 shows the corresponding moment-curvature diagrams of the beam specimens from Table 1. The black lines correspond to the first loading stage results; the green lines describe the beams' outcomes during the second loading stage (after exposing the samples to either an open environment or laboratory conditions). The looping branch of the diagram corresponds to the repeated loading for generating the stiffness decay analysis dataset. Finally, the red line defines the so-called 'service' moment, which specifies the stiffness values used to analyse the time-dependent alteration of the mechanical performances. Figure 6 shows the equivalent stress-strain diagrams transformed from the moment-curvature relationships (Fig. 5) using Equations 5a and 5b. The line colours remain the same, as Figure 5 assumes. Figure 7 illustrates the stiffness decay after repeated tests.

As equations (3b)–(5a) demonstrate, the equivalent stress calculations do not require loading history knowledge. In other words, the analysis only needs a particular moment and curvature values pair to calculate the equivalent stress. Thus, the stiffness decay analysis employs the curvature values, which belong to the ascending diagram branch corresponding to the service moment indicated in Figure 5. The loading procedure included five repetitions looping the moment-curvature diagrams within the service load range. Consequently, each test generated five loading points, i.e. the very first load was skipped to avoid the regression skewness because of excessive stiffness of the beam experiencing the first load. Figure 7 shows these points for each of the two considered loading stages. The corresponding regression line highlights the stiffness decay tendency.

The analysis of the trend lines in Figure 7 reveals a detectable decay of the material performance in beam B11 representing the NSM system and exposed to the open environment. On the other hand, beam B5 demonstrates a less evident tendency—the corresponding determination coefficients (R^2) demonstrate that the environmental exposition can explain 24.3% and 15.2% of the observed equivalent stress scatter. This result could associate the stiffness decrease to degradation of the adhesive bond, which total area is significantly higher in the EBR regarding NSM (compare 0.2 m^2 and 0.056 m^2). Thus, the expected result is that the specimen stored in the laboratory (B1) and the beam with steel reinforcement (B19) demonstrate no noticeable stiffness degradation. At the same time, the authors want to point out the illustrative nature of the presented results. This research will last for several years, and the repeated tests reveal more meaningful outcomes, and the proposed methodology will help quantify the stiffness degradation.

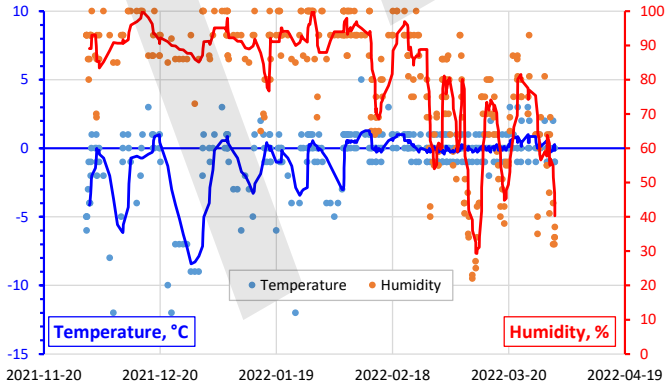

Fig. 4 The environmental conditions measured outside the laboratory building.

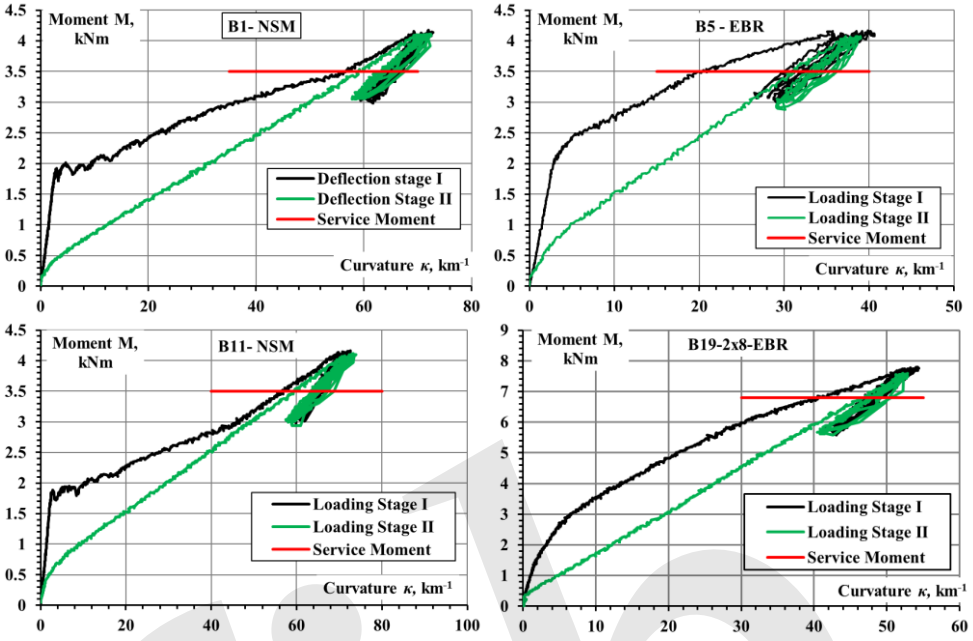

Fig. 5 The moment-curvature diagrams of the beams listed in Table 1.

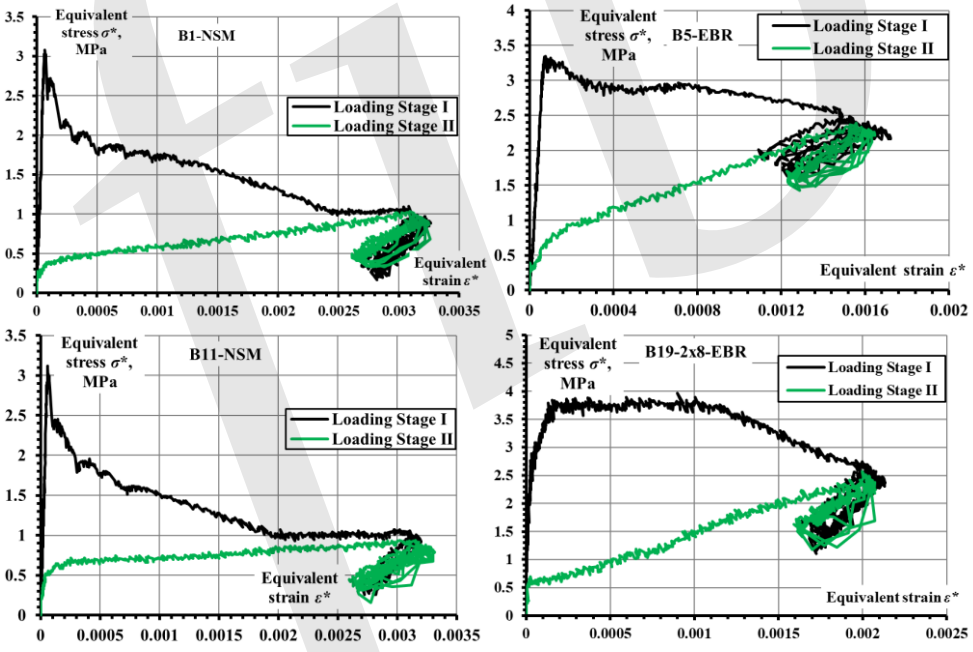

Fig. 6 The equivalent stress-strain diagrams corresponding to the moment-curvature relationships shown in Figure 5.

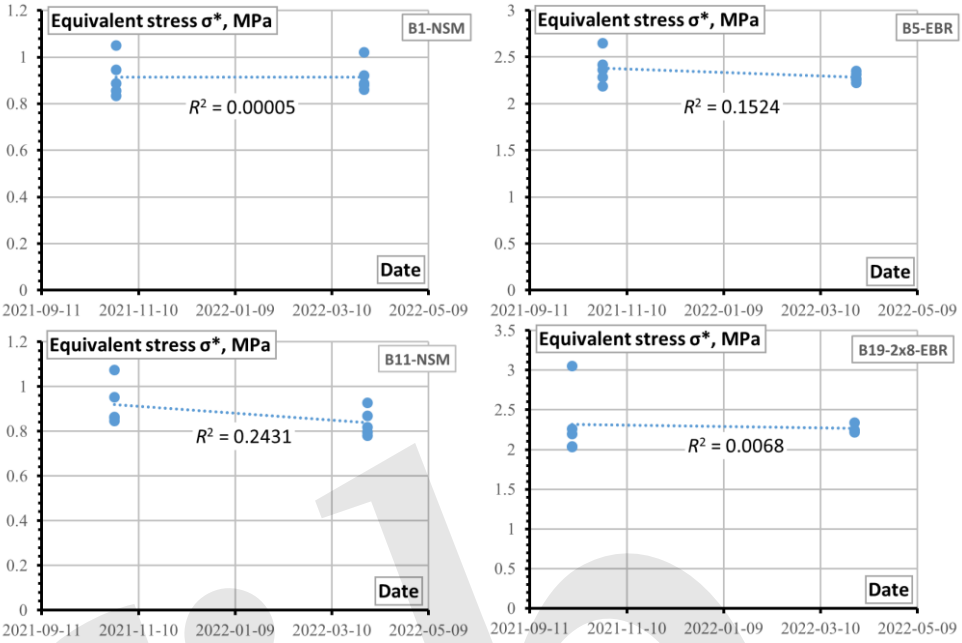

Fig. 7 The equivalent stress tendencies corresponding the 'service' moment shown in Figure 5.

5 Conclusions

This work introduces a new testing and analysis methodology for investigating the long-term degradation of concrete beams with composite strengthening systems, combining different reinforcement components. The manuscript reports partial results of the ongoing test program, which employs 34 slab-shaped beam specimens. This illustrative study includes four selected beam samples subjected to the four-point bending and achieves the following significant conclusions:

- The proposed testing layout ensures the adequacy of the simplifying assumption of the rectangular distribution shape of the stresses in the tensile concrete, which estimates the equivalent stresses in the concrete. However, this simplified theoretical model does not define concrete's constitutive law. The equivalent stresses only evaluate the residual flexural stiffness to compare and analyse the long-term decay in the mechanical performance of the composite reinforcement layouts.
- The illustrative analysis, employing only two consequent loading series with a half-year open-air exposition period, reveals a detectable decrease in the mechanical performance of the beam samples with near-surface mounted (NSM) carbon fibre-reinforced polymer (CFRP) strips. A lesser evident tendency is characteristic of the specimen with externally bonded reinforcement (EBR) CFRP sheets. The corresponding determination coefficients demonstrate that the environmental exposition can explain 24.3% and 15.2% of the observed equivalent stress scatter. On the other hand, the specimen stored in the laboratory and the beam with steel reinforcement demonstrate no noticeable stiffness degradation, the expected result.
- This investigation will last several years, and the proposed methodology helps quantify the stiffness degradation, deriving meaningful tendencies.

Acknowledgements

The authors acknowledged financial support received from European Regional Development Fund (Project No 01.2.2-LMT-K-718-03-0010) under grant agreement with the Research Council of Lithuania (LMTLT).

References

[1] Gribniak, Viktor. 2020. Special Issue "Advanced Composites: From Materials Characterization to Structural Application." *Materials* 13(24), Paper ID: 5820. doi:10.3390/ma13245820.

[2] Jakubovskis, Ronaldas, Gintaris Kaklauskas, Viktor Gribniak, André Weber, and Mantas Juknys. 2014. "Serviceability Analysis of Concrete Beams with Different Arrangements of GFRP Bars in the Tensile Zone." *ASCE Journal of Composites for Construction* 18(5), Paper ID: 04014005. doi: 10.1061/(ASCE)CC.1943-5614.0000465.

[3] Liu, TianQiao, Xing Liu, and Peng Feng. 2020. "A comprehensive Review on Mechanical Properties of Pultruded FRP Composites Subjected to Long-Term Environmental Effects." *Composites Part B: Engineering* 191, Paper ID: 107958. doi:10.1016/j.compositesb.2020.107958.

[4] Bazli, Milad, Armin Jafari, Hamed Ashrafi, Xiao-Ling Zhao, Yu Bai, and R. K. Singh Raman. 2020. "Effects of UV Radiation, Moisture and Elevated Temperature on Mechanical Properties of GFRP Pultruded Profiles." *Construction and Building Materials* 231, Paper ID: 117137. doi:10.1016/j.conbuildmat.2019.117137.

[5] Gribniak, Viktor, Aleksandr Sokolov, Arvydas Rimkus, Haji Akbar Sultani, Murat Can Tuncay, and Lluis Torres. 2019. "A Novel Approach to Residual Stiffness of Flexural Concrete Elements with Composite Reinforcement." Article in Proceedings of the IABSE Symposium – *Towards a Resilient Built Environment Risk and Asset Management*, 27-29 March 2019, Guimarães, Portugal. Zurich: IABSE, 46–51.

[6] Rimkus, Arvydas, Joaquim A.O. Barros, Viktor Gribniak, and Mohammadali Rezazadeh. 2019. "Mechanical Behavior of Concrete Prisms Reinforced with Steel and GFRP Bar Systems." *Composite Structures* 220:273–88. doi:10.1016/j.compstruct.2019.03.088.

[7] Gribniak, Viktor, Haji Akbar Sultani, Arvydas Rimkus, Aleksandr Sokolov, and Lluis Torres. 2021. "Standardised Quantification of Structural Efficiency of Hybrid Reinforcement Systems for Developing Concrete Composites." *Composite Structures* 274, Paper ID: 114357. doi:10.1016/j.compstruct.2021.114357.

[8] Gribniak, Viktor, Gintaris Kaklauskas, Algirdas Juozapaitis, Romualdas Kliukas, and Adas Meskenas. 2017. "Efficient Technique for Constitutive Analysis of Reinforced Concrete Flexural Members." *Inverse Problems in Science and Engineering* 25(1):27–40. doi:10.1080/17415977.2015.1135139.

[9] Dulinskas, Eugedijus, Viktor Gribniak, Gintaris Kaklauskas. 2008. "Influence of Steam Curing on High-Cyclic Behaviour of Prestressed Concrete Bridge Elements." *The Baltic Journal of Road and Bridge Engineering* 3(3):115–20. doi:10.3846/1822-427X.2008.3.115-120.

[10] Gribniak, Viktor, Gintaris Kaklauskas, Darius Bacinskas. 2009. "Experimental Investigation of Shrinkage Influence on Tension Stiffening of RC Beams." Article in Proceedings of the Eighth International Conference: *Creep, Shrinkage and Durability of Concrete and Concrete Structures* (ConCreep 8), Ise-Shima, Japan, 2008. London: CRC Press/Balkema, Taylor & Francis Group, 1:571–77.